Towards Dynamically-Favourable Quad-Rotor Aerial Robots

Paul Pounds, Robert Mahony, Joel Gresham
Australian National University, Canberra, Australia
paul.pounds@anu.edu.au, mahony@ieee.org, joel.gresham@anu.edu.au

Peter Corke, Jonathan Roberts
CSIRO ICT Centre, Brisbane, Australia
peter.corke@csiro.au, jonathan.roberts@csiro.au

Abstract

This paper outlines progress towards realising practical quad-rotor robot helicopters and, in particular, the Australian National University's 'X-4 Flyer' platform. Two challenges facing the X-4 are generating sufficient thrust and managing unstable dynamic behaviour. We address these issues with a rotor design technique for maximising thrust and the application of a novel rotor mast configuration. An aero-elastic blade design is described and its performance results are presented. A sprung teetering rotor hub that allows adjustment of the blade flapping characteristics and a quad-rotor dynamic model with blade flapping are introduced. The use of inverted rotors is shown to produce favorable stability properties for the Mark II X-4 Flyer.

1 Introduction

The X-4 Flyer design is based on the unique capabilities of four-rotor helicopters. Compared with conventional helicopters with single large rotors, quad-rotor craft can approach much closer to an obstacle without fear of rotor-strike. This makes the X-4 ideal for use indoors. The X-4 was conceived as an experimental platform for aerial robot research (fig. 1).

1.1 Motivation

A benefit of electric quad-rotor robots is their mechanical simplicity. Hobby radio control (RC) helicopters exhibit fast dynamics due to their small rotor size. To compensate for this, the RC models employ Bell-Hillier stabilizer linkages in the rotor control mechanism that act to slow the natural dynamic response of the inherent unstable oscillatory mode in helicopter dynamics. This makes it possible for humans to pilot the system. The X-4 has a total of eight moving parts and does not require the outlay in maintenance demanded by traditional helicopters.

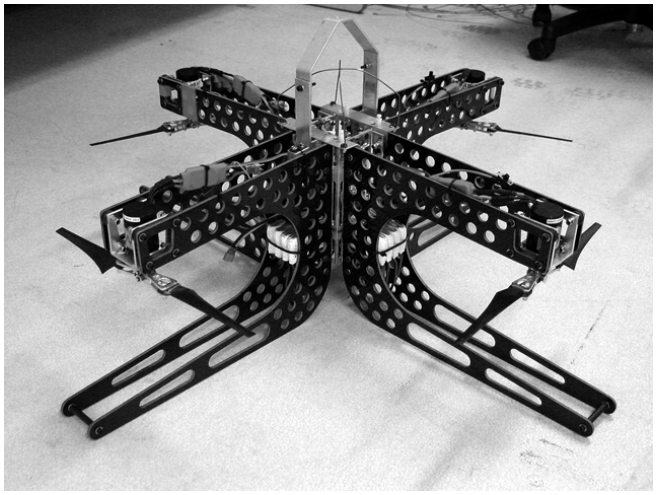

Figure 1: X-4 Flyer Mark II.

We show that the stability issues can be addressed by incorporating the effects of rotor flapping into the X-4 rotor and airframe design.

1.2 Previous Quad-Rotor Systems

One of the earliest four rotor craft was the Bréguet-Richet *Gyroplane No. 1*. The device could only attain an altitude of 1.5 m, flew for less than a minute and needed a team of men to hold it steady. It was the first full-scale rotorcraft to lift under its own power [Leishman, 2002]. The quad-rotor Bell X-22 and Curtis-Wright X-19 were part of US government initiatives to explore vertical takeoff and landing aircraft in the 1950s [Starostin, 2004]. The X-22 featured rotating ducted fans with thrust controlled by variable cyclic pitch. The X-19 much more closely resembled contemporary quad-rotor craft, although the thrust generation system was a special type of radial lift propeller.

More recently, much work has been done on quad-rotor robots. A notable development is the popular Draganflyer RC toy. The Draganflyer is the archetypical small-scale quad-rotor flyer and set the trend in current

four-rotor robots. Draganflyers have conventional rotor orientation with hingeless rotor hubs and flexible rotor blades. To offset the difficulty in flying them, the flyers have piezo-electric gyros for pitch-roll stabilisation. The simplest Draganflyers have little payload, while other models can carry a small camera.

Other similar unmanned aerial vehicles (UAV) include the Mesicopter, a micro-scale quad-rotor [Kroo *et al*, 2000]; the Hoverbot [Borenstein, 2002]; and a 'Quad-Rotor Tail-Sitter', a flyer that takes off vertically then rotates horizontally to fly on a partial wing [Young *et al*, 2002]. With the exception of the Hoverbot, all of these recent flyers have been fixed-pitch helicopters with fixed blade hubs.

1.3 Goals of Current Development

Current work on the X-4 Flyer aims to solve two problems: thrust and stability. Unlike their larger brethren, indoor helicopters have strictly limited rotor sizes, while indoor quad-rotor flyers must have smaller rotors again. The power required to hover is linked to the size of the rotor disc and so maximum lift and endurance will be dictated by the efficiency of the blade design. It is desirable to create rotors that produce the most thrust possible.

Helicopters are intrinsically unstable. They exhibit oscillating modes that are slow enough to be controlled by humans in full-scale vehicles, but these are much faster in small UAVs. The oscillatory mode is related to the rotor moment speed-stability derivative. It is possible to construct helicopters without this effect and quad-rotors are ideal for exploring this.

2 Rotors and Thrust

The rotors, motors and batteries determine the payload and flight time performance of the flyer. The rotors, especially, influence the natural dynamics and power efficiency. An approximate understanding of helicopter rotor performance can be obtained from the momentum theory of rotors. The design of the X-4 rotors draws upon the results of blade element theory for wings and helicopters.

2.1 Rotor Aerodynamics and Design Requirements

Momentum theory can be used to provide relationships between thrust, induced velocity and power in the rotor [Seddon, 1996, pp6-7]. Using energy conservation, it can be shown that in hover:

$$T = 2\rho A v_i^2 \tag{1}$$

and also:

$$P_i = \frac{T^{\frac{3}{2}}}{\sqrt{2\rho A}} \tag{2}$$

where T is the thrust produced, ρ is the density of air, A is the area of the rotor disc, v_i is the induced air velocity at the rotor and P_i is the power induced in the air.

The Figure of Merit ($F.M.$) of the rotor is the ratio of power induced in the air and power in the rotor shaft:

$$F.M. = \frac{P_i}{P_s} \tag{3}$$

This is like a rotor efficiency when calculating the theoretical onboard power requirements.

Blade element theory is particularly useful for airfoil and rotor performance. The forces and moment developed on a uniform wing are modelled by:

$$L = C_l \frac{1}{2}\rho U^2 c \tag{4}$$

$$D = C_d \frac{1}{2}\rho U^2 c \tag{5}$$

$$M = C_m \frac{1}{2}\rho U^2 c^2 \tag{6}$$

where, for unit span, L is the lift produced, D is the profile drag and M is the pitching moment [Honnery, 2000, pp94,pp112]. U is the velocity of the wing through the air and c is the chord length. C_l, C_d and C_m are non-dimensionalised coefficients of lift, drag and moment, respectively. They are dependent upon the wing's Reynolds Number (RE), Mach number and angle of attack (AoA, or α).

The RE dictates the aerodynamic conditions in which the blade operates. The RE is a dimensionless value that can be used as a measure of dynamic similarity in fluid flows. In this case:

$$RE = \frac{\rho U c}{\mu} \tag{7}$$

where here μ is the viscosity of air.

For a rotor with angular velocity ω, the linear velocity at each point along the rotor is proportional to the radial distance from the rotor shaft: $U = \omega r$. By integrating lift and drag along the length of the blade, equivalent rules may be produced for the entire rotor [Prouty, 2002, pp15]:

$$T = C_T \rho A \left(\omega R\right)^2 \tag{8}$$

$$Q = C_Q \rho A \left(\omega R\right)^2 R \tag{9}$$

where T is the total thrust produced by the rotor, Q is the rotor torque and R is the rotor radius. C_T and C_Q are non-dimensionalised thrust and rotor torque coefficients. Smaller rotors require higher speeds and more power than larger rotors for the same thrust.

For a quad-rotor helicopter weighing 4 kg with a 30 per cent control margin, each motor must produce 12.7 N of thrust. In addition, the rotor radius can be

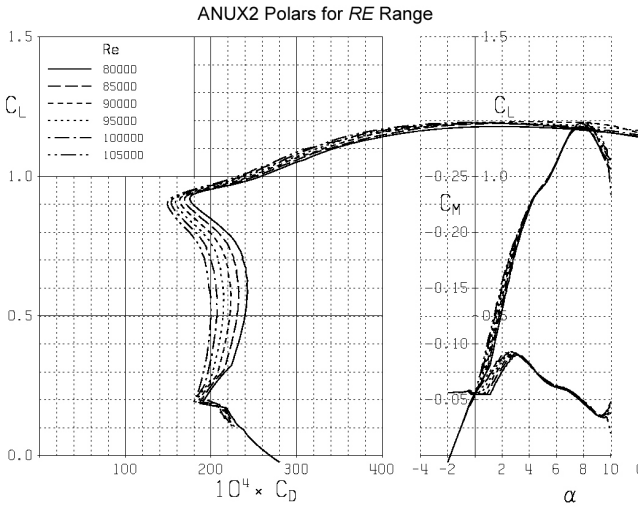

Figure 2: ANUX2 Polar Plot.

no greater than 0.165 m, due to the size of the robot, and so this will require 101.2 W of power induced in the air. The rotational velocity should be less than 800 rads^{-1} to avoid compressibility effects at the blade tip. The battery current limit of 22 A produces a maximum 0.1749 Nm motor torque and hence a top shaft power of 131 W. Therefore, the maximum theoretical thrust is 15.1 N per motor (assuming $F.M. = 1$). The actual rotor design $F.M.$ must be no less than 0.77.

The rotor design has two elements: airfoil selection and planform geometry. As the X-4 has fixed pitch, the blades are specifically optimised for hovering conditions. The aim of airfoil design is to maximise C_l and minimise C_d and C_m in the operating region of the rotor. The aim of the planform design is to set the blade dimensions so as to keep the relative AoA and RE at the ideal values for the airfoil as the linear velocity increases with radius.

2.2 Airfoil Design

At the low REs in which the blades operate (order of 100,000), very thin blade profiles at low angles of attack perform best. The DFmod3 airfoil, designed by Mark Drela for MIT's four-rotor flyer [Drela, 2003], operates at $RE = 70,000$ and has a thickness to chord ratio of 3.5 per cent. However, blades using this airfoil could not be aerodynamically scaled to suit the X-4. Thin blades are difficult to make rigid and their sharp leading edges can cause stalling at angles as low as 10°.

Changing the angle of attack alters the values of the non-dimensionalised coefficients, as shown by the familiar polar plot (fig. 2). Increasing AoA increases C_l, up to the stall angle. High-lift airfoils tend to exhibit large pitching moments. The moment is produced by the centre of lift being forward of the airfoil's geometric centre. The greater the lift produced, the greater the moment.

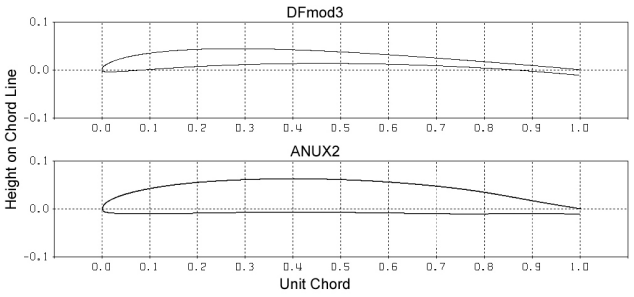

Figure 3: DFmod3 and ANUX2 Airfoil Sections, Top and Bottom.

This causes a positive-feedback, twisting effect that can lead to exceptionally thin wings, such as low-RE rotor blades, suffering severe torsional deformation.

A custom airfoil, the ANUX2, was designed using the X-foil program by Drela [Drela, 2004]. The airfoil was made twice as thick in the body as the DFmod3, with a broader nose and flat bottom surface (fig. 3). The centres of camber and thickness were also moved aft to reduce C_m. The ANUX2 was designed to operate at $RE = 94,000$ with an ideal AoA of 4.4°. In simulation the ANUX2 showed superior performance to similar high-lift, low speed airfoils such as the DFmod3, VR8 and MA409sm [NASG, 2004]. It has several favourable properties:

- Good optimal-AoA C_l of 0.9
- Insensitive to small changes in AoA
- Good performance over the operating RE range
- Improved stiffness from 7 per cent thickness ratio and increased mass at leading and trailing edges.

2.3 Planform Design for Blade Aero-elasticity

Each airfoil performs best at a specific RE and AoA. As the linear velocity changes with radius, so too must the chord length and θ vary to maintain these conditions. To keep RE constant for a given angular velocity, $c \cdot r$ must be constant.

The velocity of the air down through the rotor reduces the apparent AoA of the blades. The angle between the relative wind and the hovering blade velocity is the inflow angle, ϕ:

$$\alpha = \theta - \phi \tag{10}$$

$$\phi = \frac{v_i}{\omega r} \tag{11}$$

where θ is the geometric angle of the blades. To maintain the design AoA, the blade angle must twist such that:

$$\theta = \alpha_{ideal} + \frac{v_i}{\omega r} \tag{12}$$

These are hyperbolic distributions in r - known as 'ideal chord' and 'ideal pitch'. Although difficult to implement in full-scale helicopters, the X-4 can readily apply them.

Design for aerodynamics is complicated by blade twisting. The moment on the blades causes them to twist until either the elastic torque equals the blade pitch moment or the blade stalls. The twist along the blade is non-uniform, with the greatest deflection occurring at the blade tip. It is reasonable to only be concerned with the outboard third of the rotor, as this is where the majority of the thrust is developed. The geometric blade angle can be set so that the tip will twist up to the correct pitch.

The motor-rotor system consists of a set of dynamic interactions that reach equilibrium governed by the current available to drive the motor. An iterative simulator was coded in Matlab to find steady-states and explore the effects of design changes. The simulator uses blade element theory to determine the thrust, drag and moment produced at each radius station. Using the simulator, it is possible to test a range of reasonable parameter settings to find the ideal geometry. A similar, non-elastic method was used to design rotors for the HARVee tilt-rotor developed at the Fulton School of Engineering [Wells, 2004].

The simulator found the optimal geometry to be a tip chord of 10.4 mm, and tip pitch of 3.9°, with ideal pitch and chord. The simulator calculated a total thrust of 13.87 N at 764 rads^{-1}. The length of the blade is 165.1 mm (from the shaft centre), with the hub clamp at 40 mm. For the production blade, the tip angle was reduced to 3.1° to allow for any unexpected flex or angular error; simulation showed that variations of as much as 2° in mounting pitch error could still produce sufficient thrust. This was favourable as the screw-down mounting bracket used was not accurate to more than 0.5°.

2.4 Motors and Power

The motor-speed servo systems selected were Jeti Phasor 30-3 brushless motors, along with their companion Jeti 40-3P electronic speed controllers (ESCs). A particular advantage of this motor is the high torque performance that allows for direct drive of the rotors, rather than requiring gearing. The motors can safely pass more than 300 W at a maximum of 35 A.

The batteries used are Kokam 1500 mAh high-discharge cells. Each cell is nominally rated at 3.7 V and can deliver 12 A constantly, or 15 A for short bursts. The batteries are connected to a power bus of eight parallel sets of four cells in series; that is, 14.8 V nominal voltage and current draw of 24 A per motor.

2.5 Performance Results

As manufactured (fig. 4), the rotors produce 13.7 N of thrust on a test-rig, comparing favourably with the simulator prediction. The current draw was 22 A at 12 V at full speed. This gives the X-4 a theoretical endurance of more than eight minutes at constant full speed. At constant hovering speed, this could be extended to almost 11 minutes.

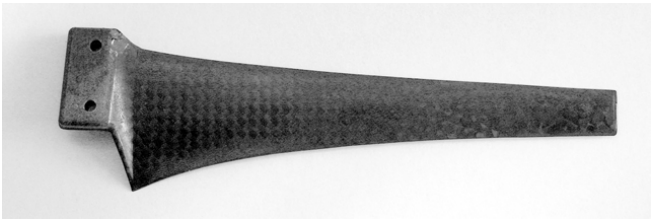

Figure 4: ANUX2 Blade With Ideal Chord and Twist.

3 Dynamics and Stability

Most treatments of quad-rotor dynamics do not include blade flapping. In fact, all rotors flap to some degree due to blade flexibility. Thin plastic rotors such as those used in the Draganflyer are particularly prone to this effect. We can model the flyer behaviour using the dynamics of a rigid-rotor quad-rotor helicopter modified with additional flapping dynamics.

3.1 Rigid Body Dynamic Model

A basic flyer dynamic model [Pounds *et al*, 2002] is modified for articulated rotors by implementing a model of the rotor flapping and generalised rotor force and torque components: $\mathcal{I}= \{E_x, E_y, E_z\}$ is a right-hand inertial frame where z is in the direction of gravity and $\xi = (x, y, z)$ is the origin of the body fixed frame $\mathcal{A} =\{E_1^a, E_2^a, E_3^a\}$. $\mathcal{A}$ is related to $\mathcal{I}$ by the rotation matrix $\mathtt{R} : \mathcal{A} \rightarrow \mathcal{I}$. V and Ω are the linear and angular velocities of the frame in $\mathcal{A}$ (fig. 5).

The revised equations are:

$$\dot{\xi} = \mathtt{R}V \tag{13}$$

$$m\dot{V} = -m\Omega \times V + mg\mathtt{R}^T e_3 + \sum_{N,S,E,W} T_i \tag{14}$$

$$\dot{\mathtt{R}} = \mathtt{R} \cdot \mathtt{sk}\left(\Omega\right) \tag{15}$$

$$\mathtt{I}\dot{\Omega} = -\Omega \times \mathtt{I}\Omega + \sum_{N,S,E,W} [Q_i + M_i] \tag{16}$$

$$\dot{\omega}_i = -\frac{1}{\tau} + \frac{K}{\tau}u_i - Q_i \tag{17}$$

$$T_i = C_T \rho A R^2 \omega_i^2 \begin{pmatrix} -s_{a_{1si}} \\ c_{a_{1si}} s_{b_{1si}} \\ c_{b_{1si}} c_{a_{1si}} \end{pmatrix} \tag{18}$$

$$Q_i = C_Q \rho A R^3 \omega_i |\omega_i| e_3 \tag{19}$$

where m and $\mathtt{I}$ are the mass and rotational inertia of the flyer, g is acceleration due to gravity, τ and K are the motor time constant and system gain, a_{1si} and b_{1si} are

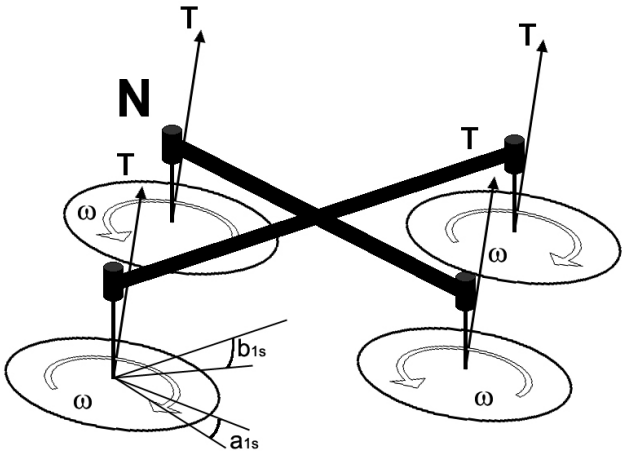

Figure 5: Flapping Quad-Rotor Free-body Diagram.

the longitudinal and lateral harmonic flapping angles of the ith rotor and M_i is the moment due to the thrust of the ith rotor.

Rotors are indexed by their corresponding compass directions: North, South, East and West ($NSEW$), where N indicates the front rotor. $\mathtt{sk}(x)$ is the skew-symmetric matrix such that $\mathtt{sk}(a)b = a \times b$ for vectors in $\Re^3$. The s_x and c_x notations represent $\sin x$ and $\cos x$ respectively.

The rotation matrix R is constructed with the yaw-pitch-roll, $\eta = (\phi, \theta, \psi)$ Euler angles:

$$\mathtt{R} = \begin{pmatrix} c_\theta c_\phi & s_\psi s_\theta c_\phi - c_\psi s_\phi & c_\psi s_\theta c_\phi + s_\psi s_\phi \\ c_\theta s_\phi & s_\psi s_\theta s_\phi + c_\psi c_\phi & c_\psi s_\theta s_\phi - s_\psi c_\phi \\ -s_\theta & s_\psi c_\theta & c_\psi c_\theta \end{pmatrix} \quad (20)$$

3.2 Blade Flapping Model

Prouty provides a generalised model for the flapping behaviour that can be adapted to the X-4 [Prouty, 2002, pp469]. The angles are described as functions of the helicopter's forward velocity and are obtained by simultaneously solving the constant and sinusoidal components of the blade centrifugal-aerodynamic-static weight moment system. For the X-4 it is presumed that the craft is moving in pure translation with no velocity component at the rotors due to yaw rotation. Application of the equations to more general flyer motion is straightforward and not done here. The flapping angle solutions for fixed pitch rotors subject to linear motion, adapted from Prouty, and Coleman's inflow model [Chen, 1990], are:

$$a_{1si} = \frac{1}{1-\frac{\mu_i^2}{2}}\mu_i\left(4\theta_t - 2\lambda_i\right) + \frac{12\left(\frac{e}{R}\right)}{\gamma\left(1-\frac{e}{R}\right)^3\left(1+\frac{\mu_i^4}{4}\right)} \times \frac{4}{3}\left(C_T/\sigma\frac{\frac{2}{3}\frac{\mu_i\gamma}{a}}{1+\frac{3}{2}\frac{e}{R}} + \mu_i\right) \quad (21)$$

$$b_{1si} = \frac{1}{1+\frac{\mu_i^2}{2}}\frac{4}{3}\left(C_T/\sigma\frac{\frac{2}{3}\frac{\mu_i\gamma}{a}}{1+\frac{3}{2}\frac{e}{R}} + \mu_i\right) + \frac{12\left(\frac{e}{R}\right)}{\gamma\left(1-\frac{e}{R}\right)^3\left(1-\frac{\mu_i^4}{4}\right)} \times \mu_i\left(4\theta_t - 2\lambda_i\right) \quad (22)$$

where e is the hinge offset, μ_i is the advance ratio of the ith rotor, a is the polar lift slope and γ is the Lock Number:

$$\gamma = \frac{\rho a c r^4}{\mathtt{I}_b} \quad (23)$$

where $\mathtt{I}_b$ is the rotational inertia of the blade about the flapping hinge.

The components of the flapping angles produced by the craft's pitch and roll rates are added to those of forward flight:

$$a_{1si} = \ldots + \frac{\frac{-\frac{16}{\gamma}\left(\frac{q}{\omega}\right)}{\left(1-\frac{e}{R}\right)^2} + \left(\frac{p}{\omega}\right)}{1-\frac{\mu_i^2}{2}} + \frac{\frac{\frac{12}{\gamma}\frac{e}{R}}{\left(1-\frac{e}{R}\right)^3}\left[\frac{-\frac{16}{\gamma}\left(\frac{p}{\omega}\right)}{\left(1-\frac{e}{R}\right)^2} - \left(\frac{q}{\omega}\right)\right]}{1-\frac{\mu_i^4}{4}} \quad (24)$$

$$b_{1si} = \ldots + \frac{\frac{-\frac{16}{\gamma}\left(\frac{p}{\omega}\right)}{\left(1-\frac{e}{R}\right)^2} + \left(\frac{p}{\omega}\right)}{1-\frac{\mu_i^2}{2}} + \frac{\frac{\frac{12}{\gamma}\frac{e}{R}}{\left(1-\frac{e}{R}\right)^3}\left[\frac{-\frac{16}{\gamma}\left(\frac{q}{\omega}\right)}{\left(1-\frac{e}{R}\right)^2} - \left(\frac{p}{\omega}\right)\right]}{1-\frac{\mu_i^4}{4}} \quad (25)$$

3.3 Rotor Moments

The moments produced by the rotor flapping are comprised of two components - the rotor hub stiffness and the thrust vector acting around a displacement from the vehicle's centre of gravity:

$$M_i = \frac{dM_M}{da_{1si}}a_{1si} + D_i \times T_i \quad (26)$$

where D_i is the rotor displacement from the flyer centre of mass:

$$D_N = \begin{pmatrix} 0 & d & h \end{pmatrix} \quad (27)$$

$$D_S = \begin{pmatrix} 0 & -d & h \end{pmatrix} \quad (28)$$

$$D_E = \begin{pmatrix} d & 0 & h \end{pmatrix} \quad (29)$$

$$D_W = \begin{pmatrix} -d & 0 & h \end{pmatrix} \quad (30)$$

d is the arm length of the flyer and h is the height of the rotors above the CoG.

The rotor stiffness, dM_M/da_{1si}, is due to physical stiffness of the rotor and centrifugal forces derived from the effective hinge offset e of the rotor. Typically, the physical stiffness of a rotor is ignored in flyer analysis and the

rotor stiffness is modelled purely as a centrifugal term. The rotor stiffness is given by Prouty as:

$$\frac{dM_M}{da_{1si}} = \frac{3}{4}\left(\frac{e}{R}\right)\frac{A_b \rho R\left(\omega R\right)^2 a}{\gamma} \tag{31}$$

In the proposed rotor design the effective hinge offset is replaced by a physical torsional spring attached to a teetering rotor. The virtual hinge offset can be calculated from the spring constant and blade centripetal behaviour. The moment about the blade flapping hinge is given by:

$$M_{C.F.} = \omega^2 \beta \left(\mathtt{I}_b + \frac{eM_b}{g}\right) \tag{32}$$

where β is the blade flapping angle and M_b is the static moment of the blade about the hinge [Prouty, 2002].

For a torsional spring of stiffness k_0 mounted at the teetering hub:

$$M_{sprg} = \omega^2 \beta \mathtt{I}_b + \beta k_0 \tag{33}$$

It can be seen that the spring will behave the same as a hinge offset, such that:

$$e_{eqv} = \frac{k_0 g}{\omega^2 \mathtt{I}_b} \tag{34}$$

The spring is not a perfect offset replacement, as the apparent offset will change with changing ω. However, around hover (near constant rotor speed) the spring will reproduce favourable hinge offset behaviour, allowing standard helicopter formulae to be applied.

3.4 Stability Analysis

By using the adapted rotor model and making some simplifications particular to the X-4, it is possible to emulate the longitudinal dynamic stability analysis by Prouty for near-hover conditions. The essential assumptions are that the advance ratio is small, the motion is constrained to pitch and X translation, the flapping angles are small and the flyer is applying the same thrust at each motor. The differential equations are given in terms of stability derivatives in X and q:

$$-m\ddot{X} + \frac{\partial X}{\partial \dot{X}}\dot{X} + \frac{\partial X}{\partial q}q - mg\Theta = 0 \tag{35}$$

$$\frac{\partial M}{\partial \dot{X}}\dot{X} - I_{yy}\dot{q} + \frac{\partial M}{\partial q}q = 0 \tag{36}$$

Using Routh's Discriminant ($R.D.$), the stability of the system can be assessed for varying physical parameters. The characteristic equation is given by:

$$s^3 - \left(\frac{1}{m}\frac{\partial X}{\partial \dot{X}} + \frac{1}{I_{yy}}\frac{\partial M}{\partial q}\right)s^2 + \frac{g}{I_{yy}}\frac{\partial M}{\partial \dot{X}} = 0 \tag{37}$$

For a cubic polynomial $As^3 + Bs^2 + Cs + D = 0$, the discriminant is $R.D. = BC - AD$. In this case:

$$R.D. \;=\; -\frac{g}{I_{yy}}\frac{\partial M}{\partial \dot{X}} \tag{38}$$

For the X-4, the stability derivatives are:

$$\frac{\partial M}{\partial \dot{X}} \;=\; 4 \times \frac{\partial M}{\partial a_{1s}}\frac{\partial a_{1s}}{\partial \mu}\frac{\partial \mu}{\partial \dot{X}} - \frac{\partial X}{\partial \dot{X}}h \tag{39}$$

$$\frac{\partial X}{\partial \dot{X}} \;=\; 4 \times -C_T \rho A\left(\omega R\right)^2 \frac{\partial a_{1s}}{\partial \mu}\frac{\partial \mu}{\partial \dot{X}} \tag{40}$$

$$\frac{\partial a_{1s}}{\partial \mu} \;=\; 4\theta_t - 2\lambda_i \tag{41}$$

$$\frac{\partial \mu}{\partial \dot{X}} \;=\; \frac{1}{\omega r} \tag{42}$$

The discriminant and coefficients provide useful information about the changing stability of the system with varying parameters [Prouty, 2002, pp602]. If $R.D.$ is positive, there will not be any unstable oscillation. Zero $R.D.$ implies neutral stability. If all characteristic equation coefficients were positive non-zero there would be no pure divergence; this is not achievable because $C = 0$. If D is zero, the system will be neutral with no oscillation. It would be ideal to set up the flyer in such a way that this final condition can be achieved.

By observation, it can be seen that neutral stability can be achieved by setting $\partial M/\partial \dot{X} = 0$. However, this requires that the rotor stiffness and thrust vector offset moments cancel and would be difficult to achieve in practice. Setting the derivative sufficiently negative ensures that the system is non-oscillatory - the helicopter will have a single unstable pole in the right-half plane which can be more easily corrected for by a human or autopilot.

For the X-4, $\partial X/\partial \dot{X}$ is always negative, while $\partial M/\partial a_{1s} \cdot \partial a_{1s}/\partial \mu$ is always positive. For pure divergence, the geometry must satisfy:

$$-C_T \rho A\left(\omega R\right)^2 h > \frac{3}{4}\left(\frac{e}{R}\right)\frac{A_b \rho R\left(\omega R\right)^2 a}{\gamma} \tag{43}$$

This can only be true if $h < 0$. Physically, this means that the centre of gravity (CoG) must be above the rotor plane. The idea of inverting the rotor not new: it has been applied in the past in De Lackner's HZ-1 [Starostin, 2004] and has similarities with the well-known Hiller Flying Platform [Starostin, 2004] and Charles H. Zimmerman's 'whirligig' [NASM, 2004]. The Mesicopter also has an inverted rotor configuration, but fixed rotors; it was found that increasing CoG distance from the rotor plane increases damping but does not benefit the natural frequency [Kroo *et al*, 2000]. In all these cases the rigid (or near-rigid) rotors would produce small or zero

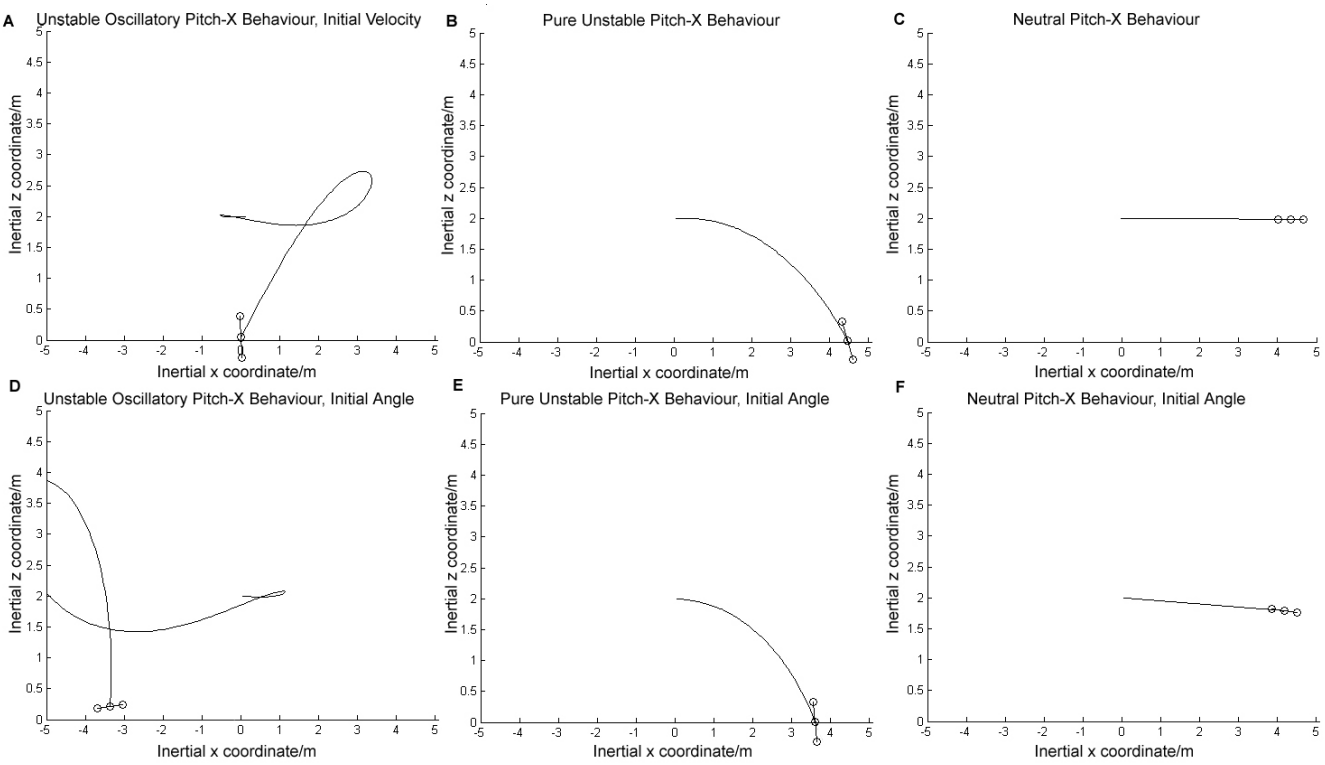

Figure 6: Simulator Dynamic Modes.

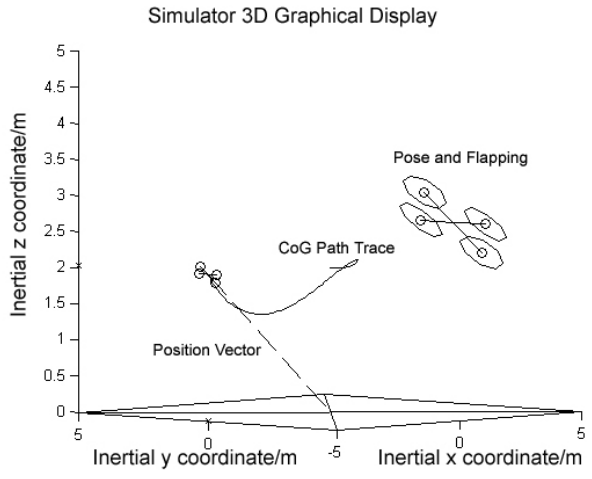

Figure 7: X-4 Flyer Simulator Graphical Output.

values for $\partial a_{1s}/\partial \mu$. The X-4 Flyer is different because it has true flapping hinges and can be adjusted into the correct dynamic mode.

4 Matlab Simulation

Before building the X-4 Flyer, a dynamic model was coded into Matlab Simulink. The simulator model is non-linear, including effects such as the flyer's rotational velocity in calculating the advance ratio per rotor. The simulator consists of three Simulink blocks: the control input mixer, output graphical display and dynamics S-Function.

The control mixer takes roll, pitch, yaw and throttle demand signals and converts them into logical $NSEW$ motor demand inputs to the dynamics block. This follows the mixing scheme outlined in Pounds [Pounds, 2002]. The same input logic is implemented on the flyer control card.

The plotter animates a schematic flyer in a 3D window (fig. 7). An attitude display shows the pose of the flyer at the current moment and a CoG trail is plotted for the total flyer motion. An additional attitude display can be turned on to show the pose and relative rotor flapping angles when the flyer moves off-screen.

The dynamics block is a Simulink M-File S-Function block. The block implements the dynamic model with continuous states for the body motion. The system is solved with an Euler ODE1 fixed step solver, with a step-size of 0.02 seconds. The simulator runs until a set time elapses or until the flyer's altitude reaches zero (crashes). The flyer parameters are entered into the dynamic model to reflect the physical hardware.

Figure 6 shows the partial state, (X, Z, q), evolution of the X-4. In each case, the initial conditions are $X = 0$m, $Z = 2$m. In the top row (A, B and C), the flyer is given

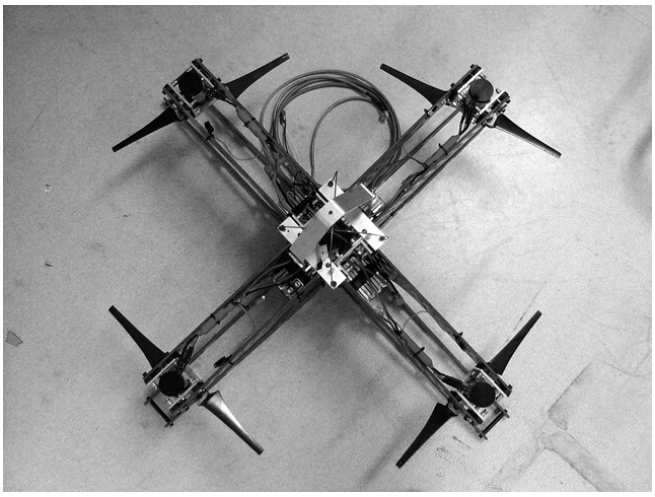

Figure 8: X-4 Flyer Layout.

Figure 9: Sprung Teetering Hub.

an initial X velocity of 0.1 ms^{-1}. In the bottom row (D, E and F), the flyer is given an initial angle of initial pitch angle of -0.1 rad. All other angles and velocities are zero and hover thrust is applied at each rotor. Columns represent changes to the mast height and hinge offset, demonstrating the different dynamic modes. In A and D, the flyer has a 20 mm equivalent hinge offset and no mast height; it exhibits unstable oscillation. In B and E the flyer has no hinge offset (teetering rotor) and -35 mm mast height; it shows pure divergence. In C and F the flyer has a 20 mm hinge offset and -13.25 mm mast height; in this case the competing derivatives cancel and produce neutral stability.

The behaviour in C and F can also be produced by setting both the mast height and hinge offset to zero; however, this is not practical for real helicopters. A pure teetering hinge does not transmit torques to the mast and so the aircraft would be uncontrollable. For making practical quad-rotor robots, the mast should be inverted and the hinge offset made small.

5 X-4 Construction and Performance

Based on the results of the stability analysis, the X-4 Flyer Mark II was built with inverted rotors in mind. From experience gained with the Mark I [Pounds, 2002], the hardware was made easier to maintain and rather than the shaft tubes of the Mark I, the flyer now has carbon fibre arms and a central frame on which to mount motors, the inertial measurement unit (IMU) and electronics.

5.1 Chassis

The X-4 has a relatively simple layout, with mounting points spaced regularly along the arms and central frame (fig. 8). This allows the CoG to be shifted above the rotor plane, rather than physically altering the mast lengths. Each arm consists of two plates connected at each end to the motor mounts and central frame. The arm plates have interior sections removed to reduce weight. The arms were cut from carbon-fibre foam sandwich sheets, but have been found to be too brittle in crashes. It is expected that these will eventually be replaced with aluminium.

The centre frame is built from aluminium sections that screw together. Angle brackets connect the arms to each section. Motors and batteries are mounted as far from the central axis as possible. Each motor screws down onto its bracket with the shaft protruding beneath. The arms angle down slightly to provide more clearance between the bottom of the arms and the tips of the rotor blades when they flap. As the motors are fixed, the batteries double as CoG ballast. Shifting the batteries higher or lower on the flyer allows the effective rotor mast height to be changed. Motor brackets fit between the arm plates.

The rotor hubs are a teetering design, machined from aluminium. A pair of torsional springs are mounting at points on each side. The torsional stiffness is adjusted by changing the springs. The blades are clamped between two plates with a pair of screws. This prevents the blade root from twisting in the mount by eliminating slop (fig. 9).

5.2 Electronics

The electronics are substantially the same as the Mark I, although a lighter sensor unit has replaced the original Crossbow IMU. The control board and 'Eimu' IMU were built by the CSIRO ICT Centre. The control board is a dual HC-12 microprocessor card with digital I/O. The Eimu is a full six-axis IMU with magnetometer [Roberts *et al*, 2003]. It is operated in vertical gyro mode to obtain

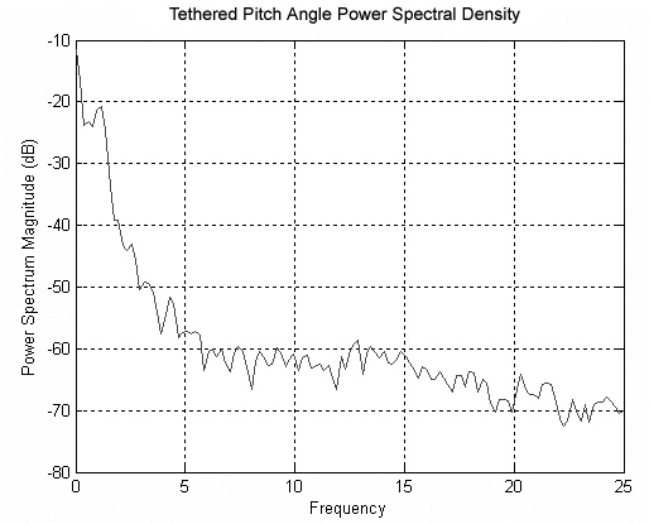

Figure 10: Logged Tethered Pitch Data Power Spectral Density.

inertial frame reference angles. There is room inside the frame for mounting the Eimu as close to the centre of gravity as possible.

Rubber grommets isolate the IMU from vibrations transmitted along the frame. Additional grommets also isolate the frame from the motors. Testing of the flyer on a tethered mount at full rotor speed showed that the IMU is relatively free from vibration. The power spectral density shows that the Eimu's filters do not pass any high-frequency noise (fig. 10). The Mark I flyer was especially susceptible to resonance in the pitch direction.

Unlike the Mark I, the Mark II incorporates simple onboard proportional-integral-derivative control. The previous iteration used a slow, off-board control system connected to the flyer by a tether. It is anticipated that the convenient aerodynamics of the X-4 will make sophisticated control unnecessary. In conjunction with onboard power, this will allow the flyer to be entirely self-contained.

6 Conclusion

The two key challenges facing the development of the Australian National University's X-4 Flyer were thrust generation and dynamic stability. The thrust generation problem was solved by developing an efficient rotor matched to the motor speed, torque and materials strength. Although free-flight experimental results are not yet available, simulation in Matlab shows that the inverted rotor configuration is beneficial to quad-rotor flyers. The X-4 Flyer has been assembled and demonstrated significant thrust. It is expected that it will exhibit slow unstable dynamics and be straight-forward to control by a human or autopilot.

7 Acknowledgements

This work was supported by Discovery grant DP0342849. The authors would like to thank

- The CSIRO ICT group for hosting and laboratory space; in particular, Leslie Overs, Stephen Brosnan and Dirk Stauffacher for their help with the flyer code and electronics.
- Joel McDonald for his work with flyer data systems.
- Mark Drela for his assistance with airfoil design

References

[Borenstein, 2002] J. Borenstein. *Hoverbot: An Electrically Powered Flying Robot*. Unpublished paper, 2002.

[Chen, 1990] R. T. N. Chen. *A Survey of Nonuniform Inflow Models for Rotorcraft Flight Dynamics and Control Applications*. In *VERTICA*, Vol. 14, No. 2, 1990.

[Drela, 2003] M. Drela. MIT 16.82 Flight Vehicle Engineering Course Demonstrator. http://student.mit.edu/catalog/m16b.html, 2004.

[Drela, 2004] M. Drela. X-Foil Subsonic Airfoil Development System. http://raphael.mit.edu/xfoil/, August 2004.

[Honnery, 2000] D. Honnery. Introduction to the Theory of Flight. Gracie Press, Northcote, Victoria, 2000.

[Kroo *et al*, 2000] I. Kroo, F. Prinz, M. Shantz, P. Kunz, G. Fay, S. Cheng, T. Fabian, C. Partridge. *The Mesicopter: A Miniature Rotorcraft Concept Phase II Interim Report*. Stanford University, July 2000.

[Leishman, 2002] J. G. Leishman. *The Bréguet-Richet Quad-Rotor Helicopter of 1907*. www.enae.umd.edu/AGRC/Aero/Breguet.pdf, May 2002.

[NASG, 2004] Nihon University Aero Student Group. *Airfoil Database*. www.nasg.com/afdb/index-e.phtml, August 2004.

[NASM, 2004] National Air and Space Museum. *Zimmerman Flying Platform "Whirligig"*. www.nasm.si.edu/research/aero/aircraft/zimmerman.htm, August 2004.

[Pounds, 2002] P. Pounds. Design, Fabrication and Control of a Four-Rotor Aerial Robot. Australian National University undergraduate thesis, Canberra, Australia, 2002.

[Pounds *et al*, 2002] P. Pounds, R. Mahony, P. Hynes and J. Roberts. *Design of a Four-Rotor Aerial Robot*. In *Proc. of Australasian Conference on Robotics and Automation*, Auckland, New Zealand, 2002.

[Prouty, 2002] R. W. Prouty. Helicopter Performance, Stability, and Control. Krieger Publishing Company, 2002, reprint with additions, original edition 1986.

[Roberts *et al*, 2003] J.M. Roberts and P.I. Corke and G. Buskey. *Low-Cost Flight Control System for a s Small Autonomous Helicopter*. In *Proceedings of IEEE Int. Conf. on Robotics and Automation*, Taipai, 2003.

[Starostin, 2004] M. Starostin. *All the World's Rotorcraft*. http://avia.russian.ee, August 2004.

[Seddon, 1996] J. Seddon. Basic Helicopter Aerodynamics. Blackwell Science, Osney Mead, Oxford, 1996.

[Wells, 2004] V. Wells. *Propeller*. www.eas.asu.edu/~harvee/papers/propeller.pdf, August 2004.

[Young *et al*, 2002] L.A. Young, E.W. Aiken, J.L. Johnson, R. Demblewski, J. Andrews, J. Klem. *New Concepts and Perspectives on Micro-Rotorcraft and Small Autonomous Rotary-Wing Vehicles*. Ames Research Center, Moffett Field, California, 2002.